Porosity-induced blueshift of photoluminescence in CdSe

E. Monaico, V. V. Ursaki, I. M. Tiginyanu, Z. Dashevsky, V. Kasiyan, and Robert W. Boyd

Citation: Journal of Applied Physics **100**, 053517 (2006); doi: 10.1063/1.2338833
View online: https://doi.org/10.1063/1.2338833
View Table of Contents: http://aip.scitation.org/toc/jap/100/5
Published by the American Institute of Physics

Porosity-induced blueshift of photoluminescence in CdSe

E. Monaico, V. V. Ursaki,[a] and I. M. Tiginyanu
National Center for Materials Study and Testing, Technical University of Moldova, Chisinau MD-2004, Moldova and Laboratory of Low-Dimensional Semiconductor Structures, Institute of Applied Physics, Academy of Sciences of Moldova, Chisinau MD-2028, Moldova

Z. Dashevsky and V. Kasiyan
Department of Materials Engineering, Ben-Gurion University of the Negev, Beer-Sheva 84105, Israel

Robert W. Boyd
Institute of Optics, University of Rochester, Rochester, New York 14627

(Received 13 May 2006; accepted 14 June 2006; published online 13 September 2006)

Porous CdSe layers have been fabricated by anodic etching of *n*-type single crystalline substrates with different values of conductivity. The morphology and porosity of the layers thus produced were found to be controlled by the conductivity of the material, anodization voltage, and conditions of *in situ* UV illumination. The porosity-induced changes in the photoluminescence spectra were studied. The decrease of the skeleton size down to 10–20 nm was found to result in a blueshift of the excitonic emission lines by 10 meV which was attributed to quantum-size effects in the nanocrystalline CdSe porous skeleton. An increase of the exciton–LO-phonon interaction by a factor of 1.5 in a weak-to-intermediate confinement regime was deduced from the analysis of temperature dependence of the free exciton luminescence line. © *2006 American Institute of Physics*.
[DOI: 10.1063/1.2338833]

INTRODUCTION

It is well known that material properties may be engineered by nanostructuring, i.e., by tailoring the architecture of macroscopic structures on the nanometer scale. Electrochemistry offers an accessible and cost-effective approach for tailoring the architecture of semiconductor materials on the submicrometer scale simply by "drilling" pores in bulk crystals and epilayers. The architecture of pores may be designed for the purpose of manufacturing integrated waveguides, Bragg-like mirrors, beam splitters, rotators of light polarization, etc.[1] Due to giant fluctuations of the electric field of electromagnetic radiation, nanoporous structures show fascinating nonlinear optical behavior, in particular, strongly enhanced second harmonic generation and terahertz emission.[2] Apart from these one-component nanostructures, porous semiconductors represent suitable templates for the fabrication of nanocomposites via filling the pores with other inorganic and organic materials including conducting polymers, which considerably extends the possibilities for developing light emitting devices and hybrid solar cells. When the characteristic dimensions of the porous skeleton entities correlate with or are much smaller than the wavelength of the electromagnetic radiation, a strong diffuse scattering of light takes place in the nanocomposite leading to the onset of light localization.[3] Because of the nanoscale nature of light absorption and photocurrent generation in solar energy conversion, the advent of methods for controlling inorganic materials on the nanometer scale opens opportunities for the development of future generations of solar cells.[4] Apart from that, doping of nanoporous II–VI materials with transition metals[5] opens prospects for the elaboration of midinfrared random lasers.

Even more spectacular changes in the material properties occur when the dimensions involved are comparable to or lower than the exciton Bohr radius. In this case, the quantum-size effects on free carriers give rise to a band gap increase of the semiconductor and sharp modification of optical and electrical properties.

Over the last decade, systematic study of porous Si and porous III–V compounds was undertaken. At the same time less attention has been paid to porous II–VI semiconductor compounds. Note that the effect of photoetching on photoluminescence (PL) of *n*-CdSe was studied many years ago,[6] but the authors interpreted the results in terms of the formation of etch pits rather than pores. Formation of porous network in a *p*-type II–VI material, namely, in *p*-$Cd_{1-x}Zn_xTe$, was demonstrated by Erne *et al.*[7,8] Recently we succeeded in introducing pores into *n*-type CdSe,[9] and we observed gain of luminescence in porous regions characterized by strong light scattering.[10] In this article, we show the possibility of introducing arrays of parallel pores with diameters as low as 10–20 nm into highly conductive *n*-CdSe single crystals. Porosity-induced blueshift of exciton bands in PL spectra of *n*-CdSe is also reported.

EXPERIMENTAL DETAILS

Wurtzite-phase *n*-CdSe single crystals were grown by chemical transport techniques. Two types of samples with the free electron concentrations of 3×10^{17} and 2×10^{18} cm^{-3} at 300 K were used in experiments. Electrochemical etching of samples with the dimensions of $5\times5\times2$ mm^3 was carried out in 5% HCl aqueous solution at room temperature under

[a]Author to whom correspondence should be addressed; electronic mail: ursaki@yahoo.com

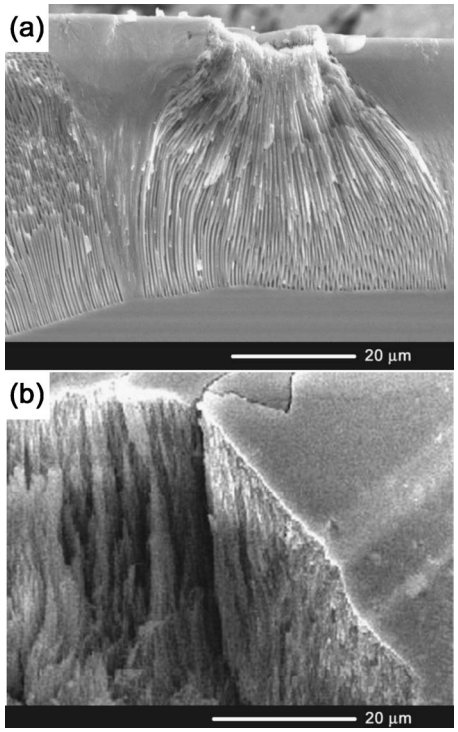

FIG. 1. SEM images taken in cross section from a CdSe sample with a free electron concentration of 3×10^{17} cm^{-3} anodized in the dark (a) and under *in situ* UV illumination (b).

potentiostatic conditions as described elsewhere.[11] The morphology and the chemical composition microanalysis of etched samples were studied using a TESCAN scanning electron microscope (SEM) equipped with an Oxford Instruments INCA energy dispersive x-ray (EDX) system. PL was excited by the 514 nm line of an Ar^+ Spectra-Physics laser and analyzed through a double spectrometer. The resolution was better than 0.5 meV. The samples were mounted on the cold station of a LTS-22-C-330 cryogenic system.

RESULTS AND DISCUSION

The top surface of *n*-CdSe samples subjected to anodic etching in the dark looks like that of the as-grown ones. In SEM images, however, one can easily identify etching pits. The analysis shows that etching starts at surface imperfections and proceeds underneath the surface along the current lines, sometimes leaving nonporous regions near the initial surface in between the etching pits [Fig. 1(a)]. Under *in situ* ultraviolet (UV) illumination by a 200 W Xe lamp focused onto the *n*-CdSe surface exposed to electrolyte, rather uniform pitting of the top surface takes place. This leads to the formation of a homogeneous porous region underneath the initial surface, it being covered by the nucleation layer with the thickness of about 3 μm, see Fig. 1(b). According to the results of EDX analysis, the composition of the porous skeleton is stoichiometric. The characteristic sizes of the skeleton and pores are controlled by the electrochemical conditions of dissolution and depend on the free carrier concentration in the initial material. The smallest characteristic size at uniform distribution of pores reached in samples with the free electron concentration of 3×10^{17} cm^{-3} is around 200 nm.

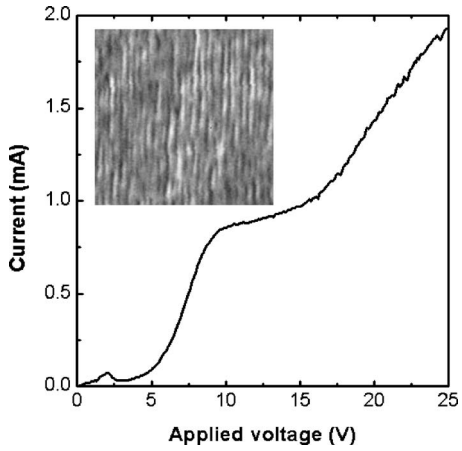

FIG. 2. Polarization curve of a CdSe sample with a free electron concentration of 2×10^{18} cm^{-3} anodized in the dark. Inserted is a SEM image with the sizes of 500×500 nm^2 taken in cross section from a sample anodized at 6.5 V.

In order to decrease the characteristic size of the porous skeleton, it is necessary to subject to anodic etching samples with higher conductivity. We explored *n*-CdSe samples with the free electron concentration of 2×10^{18} cm^{-3} for this purpose. Note that a uniform pitting of the top surface occurs in these samples without use of *in situ* UV illumination. The polarization curve measured for such specimens (Fig. 2) shows that the formation of pores starts at voltage around 5 V. The characteristic size of the obtained porous structure can be changed by the applied voltage. This parameter deduced from the statistical analysis of the SEM image of the porous structure formed at voltages slightly higher than the threshold voltage is around 10–20 nm (insert in Fig. 2). The characteristic sizes of the porous skeleton increase up to around 50 nm with the increase of the applied voltage up to 15 V (Fig. 3).

As previously reported,[9] the PL spectrum of the porous layer prepared on *n*-CdSe substrates with the free electron concentration of 3×10^{17} cm^{-3} is similar to that of the initial material when excited at a lower power density. In this paper we will focus on the investigation of changes in PL spectra introduced by porosity at characteristic sizes of the porous skeleton as low as 10–20 nm obtained on the basis of *n*-CdSe substrates with the free electron concentration of 2

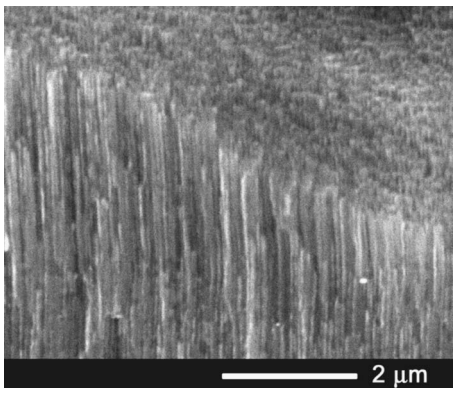

FIG. 3. SEM image of a CdSe sample with a free electron concentration of 2×10^{18} cm^{-3} anodized in the dark under the applied voltage of 15 V.

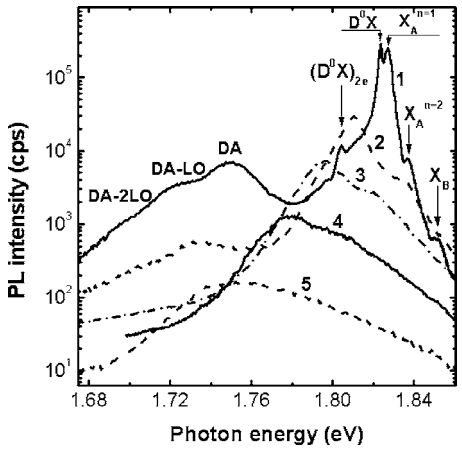

FIG. 4. PL spectrum of the *n*-CdSe crystalline substrate with a free electron concentration of 2×10^{18} cm^{-3}. Temperatures (K) of (1) 10, (2) 100, (3) 150, (4) 200, and (5) 300.

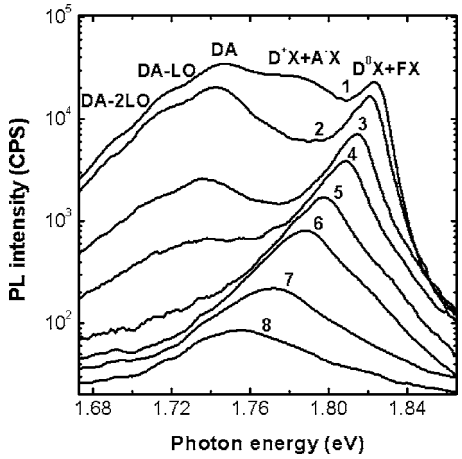

FIG. 5. PL spectrum of the *n*-CdSe sample anodized in the dark under an applied voltage of 15 V. Temperatures (K) of (1) 10, (2) 40, (3) 70, (4) 90, (5) 120, (6) 150, (7) 200, and (8) 250.

$\times10^{18}$ cm^{-3}. The PL spectrum of the as-grown CdSe single crystals with the free electrons concentration of 2×10^{18} cm^{-3} measured at 10 K (see Fig. 4) is dominated by the PL bands related to the recombination of neutral donor bound excitons (D^0X) at 1.823 eV and free X_A excitons at 1.827 eV. On the high-photon-energy side of these bands, luminescence related to the excited state of the X_A exciton at 1.837 eV and of the X_B exciton at 1.851 eV are observed. An effective Rydberg constant of the X_A exciton equal to 13 meV is deduced from these data. This exciton binding energy along with the X_A exciton series limit of 1.840 eV and the $\Gamma_9-\Gamma_7$ valence band crystal field splitting of 24 meV corroborate the previously reported data.[12] On the low-photon-energy side of the (D^0X) peak, one can find two-electron replica $(D^0X)_{2e}$ at 1.804 eV. The (D^0X) peak is due to the radiative decay of the excitons bound to a neutral donor with the liberation of free excitons and leaving the donor in the ground state. The separation of 4 meV between the (D^0X) and X_A peaks is the binding energy of the exciton to the neutral donor. The two-electron replica results from the recombination of the excitons bound to the neutral donor, the donor being left in an excited state. The energy of the $(D^0X)_{2e}$ is therefore lower than that of the principal (D^0X) peak by the difference in ground and excited state energies. The binding energy of the donor involved can be estimated using a simple hydrogen model, where the binding energy is just 4/3 of the separation between the (D^0X) and $(D^0X)_{2e}$ peaks. According to the Haynes rule, the excitonic localization energy scales linearly with the donor binding energy $[E_{\text{bind}}(D^0X)=bE_{\text{donor}}]$, with the constant b in the range of 0.1–0.3 for different semiconductors. A value of b equal to 0.17 is deduced from our experiments. Apart from excitonic luminescence, a much weaker PL band associated with donor-acceptor (DA) recombination[9,10,13] along with phonon replica is inherent to the as-grown material. With the temperature increase, the luminescence related to donor bound excitons sharply decreases, and at temperatures higher than 50 K the luminescence is free excitonic.

The luminescence related to the recombination of neutral donor bound excitons and free excitons is considerably reduced in the porous layer produced with applied voltage of 15 V during dissolution, and the PL spectrum is dominated by the DA recombination (see Fig. 5). At the same time, a broad PL band emerges in the spectrum at photon energies around 1.79 eV. We attribute this band to the recombination of excitons bound to ionized donors and acceptors formed during dissolution at high applied voltages. The sharp quenching of this luminescence similar to that of the luminescence related to the recombination of neutral donor bound excitons with the temperature increase up to 40–50 K is an argument supporting this suggestion.

In contrast to the as-grown material and the porous material produced at high applied voltage, the luminescence of the nanostructured material obtained at low applied voltage during the dissolution process is dominated by free exciton recombination starting from temperatures as low as 10 K (see Fig. 6). The other two features of the PL from the porous material are the blueshift of the excitonic emission by 10 meV and a higher intensity of the LO phonon replica of the X_A exciton. Apart from excitonic luminescence, the DA related luminescence is observed in PL spectra at temperatures up to 100 K. At temperatures above 100 K, the DA luminescence sharply decreases, since the impurity with

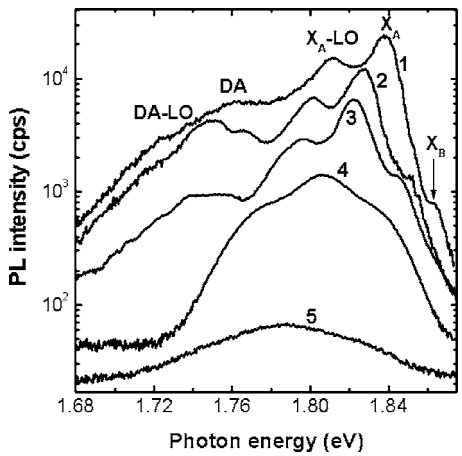

FIG. 6. PL spectrum of *n*-CdSe sample anodized in the dark under an applied voltage of 6.5 V. Temperatures (K) of (1) 10, (2) 70, (3) 100, (4) 150, and (5) 200.

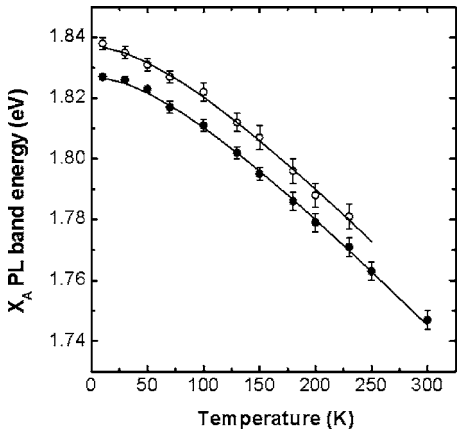

FIG. 7. Temperature dependence of the X_A exciton line energy in CdSe crystalline substrate (full symbols) and porous layer anodized at 6.5 V (open symbols). Lines represent the fit of the experimental data to the Varshni formula.

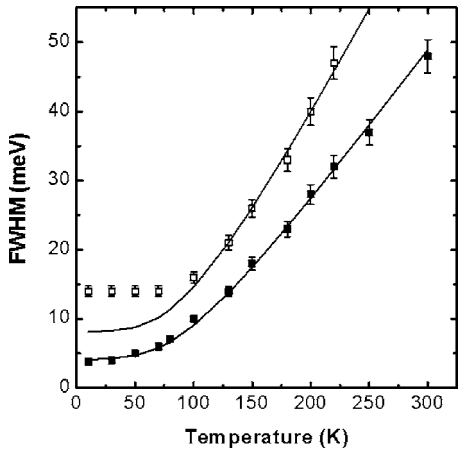

FIG. 8. Temperature dependence of the FWHM of the X_A exciton line in CdSe crystalline substrate (full symbols) and porous layer anodized at 6.5 V (open symbols). Lines represent the fit of the experimental data to the theoretical equations.

smaller binding energy involved in DA transitions (most probably the donor impurity) is ionized. At the same time, a high-energy shoulder of the DA band associated with free-to-bound transition becomes resolved in the spectra at temperatures above 50 K.

The temperature dependence of the X_A exciton energy in the as-grown material (Fig. 7) is well fitted with the phenomenological Varshni formula[14]

$$E(T) = E_0 - \alpha T^2/(T+\beta), \tag{1}$$

with the parameters $E_0 = 1.837$ eV, $\alpha = 4 \times 10^{-4}$ eV K^{-1}, and $\beta = 140$ K.

The deduced values of the α and β parameters are in reasonable coincidence with the previously reported data.[15,16] The temperature dependence of the X_A exciton energy in the nanostructured material is well fitted with the same parameters but with the value of $E_0 = 1.837$ eV which is 10 meV higher than that of the as-grown material. We attribute this blueshift to the quantum-size effects in the nanocrystalline porous skeleton. It is well known that the optical properties of nanocrystals strongly depend on the ratio of the nanocrystal size a to the Bohr radius of the bulk exciton a_B. In the analysis of the experimental data, one needs to consider three different regimes: $a \gg a_B$, $a \sim a_B$, and $a \ll a_B$. The exciton Bohr radius in CdSe is around 5 nm.

In the case $a \gg a_B$, the binding energy of an exciton is larger than the quantization energy of both the electron and holes, and the optical spectra of these nanocrystals are determined by the quantum confinement of the exciton center of mass.[17] In this case the quantum confinement blueshift of the exciton energy is given by $h^2/(8Ma^2)$, where $M = m_e + m_h$ is the exciton translation mass. This case is known as the weak confinement regime. The strong confinement regime is realized in small nanocrystals, where $a \ll a_B$. In this case, the exciton translation mass is replaced by the exciton reduced mass $\mu^{-1} = m_e^{-1} + m_h^{-1}$ in the above presented formula. By using the values of the free carrier effective masses of $m_e = 0.13 m_0$ and $m_h = 0.45 m_0$, one can calculate a blueshift of around 6 meV in the case of weak confinement regime and a shift of 30 meV in the case of strong confinement regime in CdSe nanocrystals with the average size of 10 nm. The experimentally observed shift of 10 meV in our nanostructured layer suggests that we deal with a case of weak-to-intermediate confinement regime.

The higher intensity of the LO phonon replica of the X_A exciton in nanostructured layer as compared with that inherent to the as-grown material is indicative of a stronger exciton–LO-phonon interaction. The strength of the exciton–LO-phonon interaction is an important parameter since it affects optical and electrical properties of semiconductors (emission line broadening, hot carrier cooling, and carrier mobility). We investigated the influence of nanostructuring upon the exciton–LO-phonon interaction via the analysis of the X_A exciton linewidth (Fig. 8). The measured luminescence linewidth is the sum of an inhomogeneous part (Γ_i) that is due to intrinsic effects (dislocations, interface roughness, composition fluctuations, and electron-electron interactions) and a temperature-dependent homogeneous part (Γ_h). At low temperatures, the homogeneous component is dominated by the scattering of acoustical phonons. As the temperature increases, the LO phonon scattering becomes dominant due to the increase of the phonon population. The broadening due to the impurity scattering also becomes important at higher temperatures due to the ionization of impurities. The full width at half maximum (FWHM) of the emission line can be expressed through the following equations:[18,19]

$$\Gamma(T) = \Gamma_i + \Gamma_h \tag{2}$$

$$\Gamma_h = \Gamma_{\mathrm{AC}} T + \Gamma_{\mathrm{LO}}/[\exp(E_{\mathrm{LO}}/k_B T) - 1] + \Gamma_{\mathrm{imp}}/[\exp(E_{\mathrm{imp}}/k_B T)], \tag{3}$$

where Γ_{AC}, Γ_{LO}, and Γ_{imp} are interaction constants and E_{LO} and E_{imp} are the average LO phonon energy and the impurity ionization energy. By using the LO phonon energy of 26 meV and the impurity activation energy of 24 meV deduced from the $(D^0X)_{2e}$ peak position, the best fit in the as-grown material was reached with the following param-

eters: $\Gamma_i = 3.5$ meV, $\Gamma_{AC} = 1 \times 10^{-2}$ meV/K, $\Gamma_{LO} = 60$ meV, and $\Gamma_{imp} = 20$ meV.

The previously reported values of the Γ_{AC} lie in the interval of $1 \times 10^{-3} - 3 \times 10^{2}$, the value of Γ_{LO} is between 20 and 60 meV, and the value of the Γ_{imp} most commonly used is 15–20 meV.[15,16] The smallness of the inhomogeneous broadening, along with the PL spectra presented above, is indicative of the high quality of the as-grown CdSe single crystals.

In contrast with the as-grown samples, the best fit of the experimental data in the nanostructured material is reached with the Γ_{LO} value of 90 meV and the $\Gamma_i = 8$ meV. The higher value of the Γ_i is due mainly to a statistical distribution of the porous skeleton sizes, while the increased value of the Γ_{LO} by a factor of 1.5 is related to a stronger exciton–LO-phonon interaction in the nanostructured layer.

CONCLUSION

The results of this study demonstrate the possibility of preparing nanoporous CdSe templates with the characteristic size of the porous skeleton entities down to 10–20 nm by means of an accessible and cost-effective approach based on electrochemical etching of bulk crystalline substrates. We found that the dimensions of the pores and porous skeleton entities can be controlled by the conditions of the electrochemical etching. The decrease of the skeleton size down to 10–20 nm leads to a blueshift of the excitonic emission lines by around 10 meV due to quantum-size effects in a weak-to-intermediate confinement regime. The exciton–LO-phonon interaction in the nanocrystalline CdSe porous skeleton is increased by a factor of 1.5 in comparison with that inherent to bulk crystals.

ACKNOWLEDGMENT

This work was supported by the U.S. Civilian Research and Development Foundation under Grants Nos. ME2-2527 and MOR2-1033-CH-03.

[1] H. Föll, S. Langa, J. Carstensen, M. Christophersen, and I. M. Tiginyanu, Adv. Mater. (Weinheim, Ger.) **15**, 183 (2003).
[2] M. Reid, I. V. Cravetchi, R. Fedosejevs, I. M. Tiginyanu, L. Sirbu, and R. W. Boyd, Phys. Rev. B **71**, 081306 (2005).
[3] F. J. P. Schuurmans, D. Vanmaekelbergh, J. van de Lagemaat, and A. Lagendijk, Science **284**, 141 (1999).
[4] W. U. Hyunh, J. J. Dittmer, and A. P. Alivisatos, Science **295**, 2425 (2002).
[5] V. Kasiyan, Z. Dashevsky, R. Shneck, and E. Towe, J. Cryst. Growth **290**, 50 (2006).
[6] R. Garuthara, M. Tomkiewicz, and R. Tenne, Phys. Rev. B **31**, 7844 (1985).
[7] B. H. Erne, A. Million, J. Vigneron, D.-C. C. Mathieu, and A. Etcheberry, Electrochem. Solid-State Lett. **2**, 619 (1999).
[8] B. H. Erne, C. Mathieu, J. Vigneron, and A. Million, J. Electrochem. Soc. **147**, 3759 (2000).
[9] I. M. Tiginyanu, E. Monaico, V. V. Ursaki, V. E. Tezlevan, and R. W. Boyd, Appl. Phys. Lett. **86**, 063115 (2005).
[10] E. Monaico, V. V. Ursaki, A. Urbieta, P. Fernandez, J. Piqueras, R. W. Boyd, and I. M. Tiginyanu, Semicond. Sci. Technol. **19**, L121 (2004).
[11] S. Langa, I. M. Tiginyanu, J. Carstensen, M. Christophersen, and H. Foll, Appl. Phys. Lett. **82**, 278 (2003).
[12] R. G. Wheeler and J. O. Dimmock, Phys. Rev. **125**, 1805 (1962).
[13] R. Jäger-Waldau *et al.*, J. Appl. Phys. **64**, 2601 (1988).
[14] Y. P. Varshni, Physica (Amsterdam) **34**, 149 (1967).
[15] M.-C. Kuo *et al.*, Jpn. J. Appl. Phys., Part 1 **43**, 5145 (2004).
[16] O. Maksimov, W. H. Wang, N. Samarth, M. Munoz, and M. C. Tamargo, Solid State Commun. **128**, 461 (2003).
[17] Al. L. Efros and M. Rosen, Annu. Rev. Mater. Sci. **30**, 475 (2000).
[18] H. J. Lozykowski and V. K. Shastri, J. Appl. Phys. **69**, 3235 (1991).
[19] T. Li, H. J. Lozykowski, and J. L. Reno, Phys. Rev. B **46**, 6961 (1992).